separations

MDPI

Article

In Vitro and Reactive Metabolites Investigation of Metabolic Profiling of Tyrosine Kinase Inhibitors Dubermatinib in HLMs by LC–MS/MS

Nasser S. Al-Shakliah *, Adnan A. Kadi, Hatem A. Abuelizz and Rashad Al-Salahi

Department of Pharmaceutical Chemistry, College of Pharmacy, King Saud University, Riyadh 11451, Saudi Arabia
* Correspondence: nassersalem30@yahoo.com

Abstract: Dubermatinib (DMB, TP-0903), a benzenesulfonamide, is an inhibitor of the tyrosine kinase AXL, which is a member of the TAM family and can prevent GAS6-mediated activation of AXL in cancer cells. Patients with previously treated chronic lymphocytic leukemia are being studied in phase I/II clinical trials to determine its antineoplastic potential (CLL). In the current work, the Xenosite web predictor tool was employed to predict the vulnerable sites of metabolism and the reactivity pathways (cyanide and GSH) of DMB. Subsequently, we present the analysis and identification of in vitro and reactive intermediates of DMB using liquid chromatography ion trap mass spectrometry (LC–ITMS). Human liver microsomes (HLMs) were exposed to dimethylbenzene in a laboratory setting, and the resulting metabolites were collected through protein precipitation. Intense reactivity toward nucleophilic macromolecules was seen in the metabolites of the piperazine and pyrimidine rings in DMB, iminium, and 2,5-quinone-imine, respectively. To assess the toxicities of the possibly reactive metabolites, DMB was incubated with HLMs in the presence of 1.0 mM KCN and 1.0 mM glutathione. The DMB metabolites found by LC–MS/MS were seven in vitro phase I metabolites, three cyano adducts, and two GSH conjugates. Phase I in vitro metabolic reactions included *N*-demethylation, hydroxylation, and dechlorination. DMB and its metabolites have not been investigated for their metabolism in vitro.

Keywords: *N*-methyl piperazine; Dubermatinib; in vitro metabolites; cyano adducts; GSH conjugate; Xenosite reactivity model

Citation: Al-Shakliah, N.S.; A. Kadi, A.; Abuelizz, H.A.; Al-Salahi, R. In Vitro and Reactive Metabolites Investigation of Metabolic Profiling of Tyrosine Kinase Inhibitors Dubermatinib in HLMs by LC–MS/MS. *Separations* **2023**, *10*, 353. https://doi.org/10.3390/separations10060353

Academic Editor: Beatriz Albero

Received: 14 May 2023
Revised: 2 June 2023
Accepted: 7 June 2023
Published: 13 June 2023

1. Introduction

Drugs belonging to the tyrosine kinase inhibitor (TKI) class selectively inhibit kinase activity by modifying intracellular signals required for the growth of cancer cells [1]. As regulatory enzymes, tyrosine kinases (TKs) switch various cellular processes on and off by transferring gamma phosphate groups from ATP to the hydroxyl groups of target proteins [2]. Phosphorylation of proteins by kinases is a crucial signal for controlling cellular activities like cell division, and the phosphorylation of proteins often occurs at serine or threonine residues. Dubermatinib (DMB, TP-0903) inhibits tumor cell proliferation and migration by blocking AXL-mediated signal transduction pathways and so inhibiting epithelial-mesenchymal transition (EMT). Tumor cell proliferation, survival, invasion, and metastasis are all influenced by the TAM family of receptor tyrosine kinases (TYRO3, AXL, and MERTK), whose suppression results in decreased tumor cell proliferation and migration [3]. DMB is being studied in a phase I/II clinical trial in patients with previously treated chronic lymphocytic leukemia (CLL) and has been shown to inhibit tumor cell motility, survival, invasion, proliferation, colony formation, and chemotherapeutic sensitivity [4,5]. A phospho-kinase array of DMB-treated cells demonstrated an increase of greater than 50% in p53 S392 and Chk-2 T68 phosphorylation, as well as a similar increase in histone H2AX phosphorylation in a model of neuroblastoma [6]. Patients with

advanced metastatic or progressive solid tumors and acute lymphocytic leukemia (AML) are currently participating in phase I/II trials to evaluate the dosage, safety, pharmacodynamics, and pharmacokinetics of DMB (clinical trial identification numbers: NCT02729298, NCT04518345, and NCT03013998).

Liquid chromatography-mass spectrometry (LC–MS) was performed to differentiate and describe in vitro DMB metabolites. Moreover, the generated reactive metabolite(s) can covalently alter proteins, which is regarded as the initial step in producing drug-induced organ toxicities. This study was conducted to determine whether or not reactive metabolites could aid in the prediction of the toxicities of DMB and its pharmacological relatives. Mass spectrometry failed to detect reactive metabolites in vivo due to their ability to bind to endogenous components, including DNA and proteins [7]. Our team has previously investigated the production of reactive metabolites by TKIs. This work was expanded upon in the current investigation, which demonstrated that DMB generated five reactive intermediates via two distinct bioactivation pathways. The created reactive metabolites were isolated, identified, and the bioactivation pathways were determined using two distinct trapping agents. As shown in Figure 1, the *N*-methyl piperazine ring is a defining structural feature of DMB. Compounds containing this moiety were shown to be metabolically bioactivated to yield the iminium intermediates that are attacked by potassium cyanide as a nucleophile to afford the cyano adducts [8]. The halogenated benzene ring in DMB undergoes metabolic bioactivation via oxidation, resulting in the reactive intermediate 2,5-quinone-imine, which can be addressed by glutathione [9]. Liquid chromatography-mass spectrometry (LC–MS/MS) was utilized to conduct the identification and characterization of DMB in vitro metabolites. This analysis aimed to detect reactive metabolite(s) that have the potential to chemically modify proteins, representing an initial stage in the development of drug-induced organ toxicities. Thus, the investigation focused on evaluating the presence of reactive metabolites to aid in predicting toxicities associated with DMB and its related drugs. The detection of reactive metabolites in vivo is challenging due to their ability to bind to endogenous materials like DNA and proteins, which hampers their identification through mass spectrometry [10–13]. The molecular basis of DMB in vitro biotransformation and changes in the properties of the metabolites relative to the parent compound were investigated by performing in silico drug metabolism. When compared to experimental stages for metabolic and toxicity profiles, in silico methods are less expensive and take less time to complete [14–16]. The Xenosite CYP450 model was used to anticipate susceptible metabolic sites in the DMB chemical structure (Figure 1), as well as to detect the bioactive center and structural alarms in the DMB structure, both of which improved its safety and efficacy in a variety of targets.

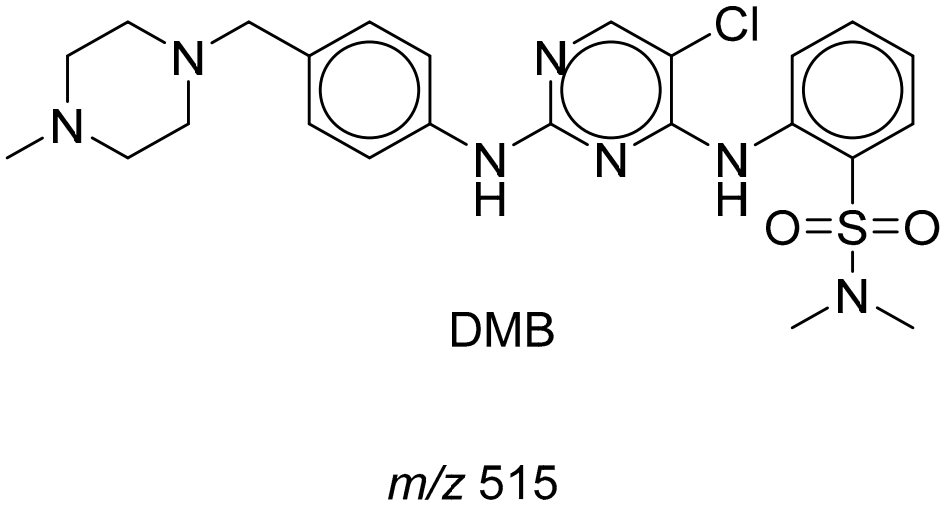

Figure 1. Chemical structure of DMB.

2. Chemicals and Methods

2.1. Chemicals

Milli-Q was connected to the Elix Millipore water purification system to obtain water (Millipore, Burlington, MA, USA). BDH laboratory supplies were the source for magnesium chloride ($MgCl_2$) and sodium hydroxide (NaOH) (Poole- Bromborough, UK). ACROS produced nicotinamide adenine dinucleotide phosphate (NADPH). WINLAB, UK supplied potassium dihydrogen phosphate (KH_2PO_4) and sodium dihydrogen phosphate (NaH_2PO_4). Sigma-Aldrich supplied glutathione reductase (GSH), acetonitrile (ACN) HPLC-grade, formic acid (HCOOH), and potassium cyanide (KCN) (St. Louis, MO, USA). The Dubermatinib (TP-0903) was acquired from Med Chem (Princeton, NJ, USA). Male liver microsomes (M0567) were obtained from the company Sigma-Aldrich (West Chester, PA, USA). The HLMs were kept at 70 °C until their use. HLMs contained 20 mg/mL of protein in a solution of 250 mM sucrose. HepaRGTM Cryopreserved Cells (HPRGC10) were purchased from ThermoFisher (Waltham, MA, USA).

2.2. Chromatographic Conditions

The separation was accomplished using an Agilent 1290 series system comprised of a G1311A quaternary pump, a G1322A degasser, a G1367B HIP–ALS autosampler, a G1316A thermostatted column compartment, and an Agilent 6320 Ion Trap mass spectrum. We employed a mobile phase of 0.1% formic acid in water (A) at a pH of 4.5 and 0.1% formic acid in acetonitrile solvent (B) in conjunction with an eclipse plus C18 (2.1 150 mm 3.5 m) column. The water/acetonitrile mixture was subjected to gradient chromatography for 85 min at a flow rate of 0.2 mL/min. When the program began, 95% of solvent A was employed, and then within 60 min, the percentage of solvent B was increased from 5% to 60% and then remained constant for the following 20 min. A 5 µL sample was fed into the HPLC apparatus. The drying gas was nitrogen, the gas temperature was 350 degrees Celsius, the gas flow was 11.0 L/min, the nebulizer pressure was 55 pounds per square inch, ESI was used as the ion source, the capillary voltage was 4000 volts, and the mode was positive in the MS.

2.3. Xenosite Web Predictor for In Silico Prediction

Available and free online software is utilized to estimate the likely metabolic locations of xenobiotics and other tiny chemical compounds. It suggests that nine key CYP450 isoenzymes, including 1A2, 2B6, 2A6, 2C9, 2C8, 2D6, 2C19, and 3A4, as well as human liver microsomes, are involved (HLM). The software has a quick runtime, and the metabolism-produced site score correlates closely with potential metabolite [17,18]. For the metabolism-produced site prediction, the DMB chemical structure in SMILES format was uploaded to the website.

In silico studies were performed using the XenoSite reactivity model, which can be downloaded for free from http://swami.wustl.edu/xenosite (accessed on 13 May 2023) to identify sites where reactive intermediate [17] might potentially cause damage. More than 680 molecules were used in neural networks to create this predicted model. The software's speedy execution time is one of its many advantages [19].

2.4. In Vitro Metabolism of DMB

Twenty HLMs from human livers were treated with DMB in a manner similar to that previously described [20]. The HLMs were prepared by adding a 0.08 M phosphate buffer to a stock solution of dimethyl benzene in dimethyl sulfoxide (DMSO) (pH 7.4). To begin, the components were shaken together in a water bath preheated to 37 degrees Celsius for 5 min to ensure that they were well-mixed. The incubation procedure was initiated with a solution of nicotinamide adenine dinucleotide phosphate (NADPH). In a final incubation mixture volume of 1 mL, the drug concentration was 30 M, the NADPH concentration was 1 mM, and the microsomal protein concentration was 1 mg/mL. NAPDH was substituted with a buffer solution, and the microsomal protein was used as a positive

control. After 90 min of incubation, 2 mL of ice-cold acetonitrile was added to end the reaction and precipitate the proteins. Next, the samples were centrifuged at 21,900× *g* for 10 min. Re-containerization and evaporation of the supernatant in a stream of nitrogen. After reconstituting the residue in the mobile phase, it was sent to vial HPLC for analysis. In order to catch reactive intermediate metabolites, an identical procedure was carried out with either 1.0 mM glutathione (GSH) or 1.0 mM KCN. Negative controls were tested using the same procedures as positive controls to ensure reliability. The activity of the microsomal preparation was measured against a concentration of phenytoin (2 M).

3. Results and Discussion

3.1. DMB Metabolism and Reactivity (In Silico Prediction)

DMB SOMs suggested the most essential isoenzymes of CYP450, which include 1A2, 2A6, 2B6, 2C8, 2C9, 2C19, 2D6, 2E1, 3A4, and HLM. The outcomes of DMBs in silico site of metabolism (SOM) predictions are displayed in Figure 2. The results were presented graphically, with details such as the strength of the color gradient and the bar representing the color scale. The greatest possible SOM score for a given atomic site is 1; hence a red color suggests a high probability of metabolism at that site, whereas a white color indicates no metabolism at that location. Two methyl groups of sulphonamide, *N*-methyl-piperazine, and carbons linked to the nitrogens of piperazine have been identified as possible atomic sites for metabolism in the DMB structure. These results agreed with experimental work that measured seven in vitro phase I metabolites (M1-M7), as well as cyano adducts and GSH conjugates.

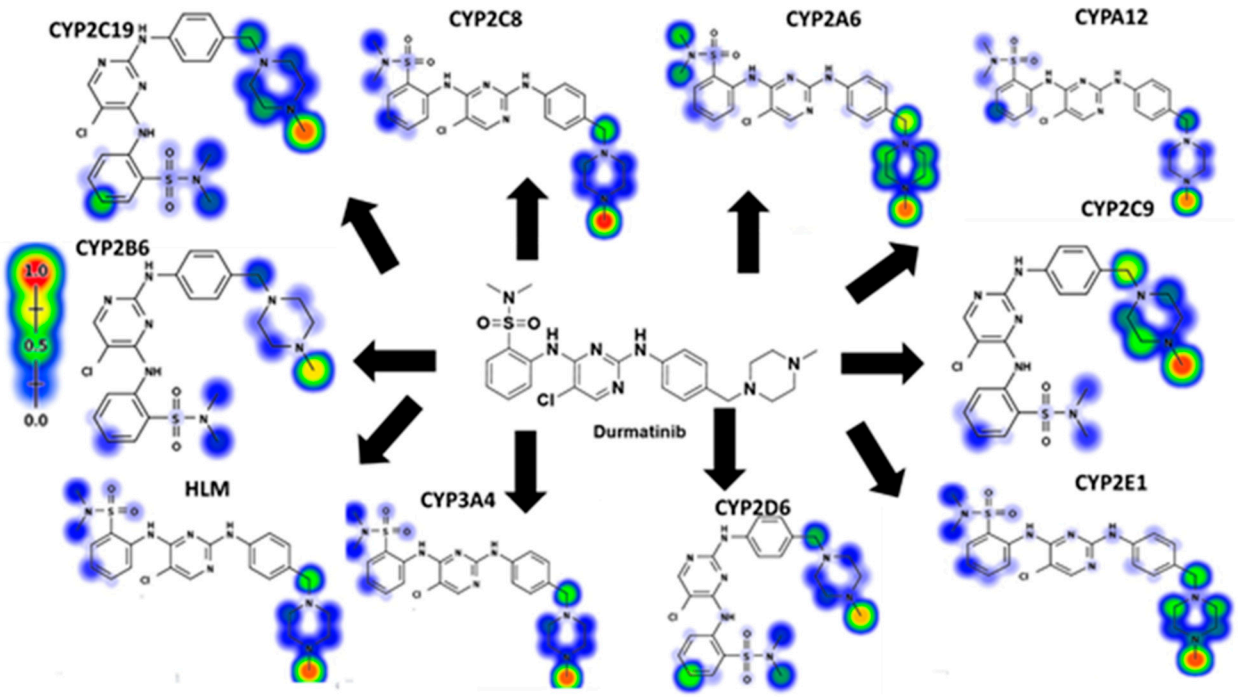

Figure 2. Predicted atomic sites of DMB metabolism by Xenosite web predictor.

Figure 3 displays the results of the Xenosite web page's cyano and GSH model's prediction of DMB reactivity. This effort was directed by a list of proposed metabolites and reactive intermediates that was generated using in silico hypotheses and previous knowledge from the literature. The cyano reactivity model predicts the most probability of *N*-methyl-piperazine and the carbons connected to piperazine nitrogens, while the GSH reactivity model predicts the highest chance of 5-chloropyrimidine bioactivation, which are in consistent agreement between experimental findings and theoretical calculations

of reactivity. As the color's intensity suggests, other potential bioactivation sites are not particularly high on the list of priorities.

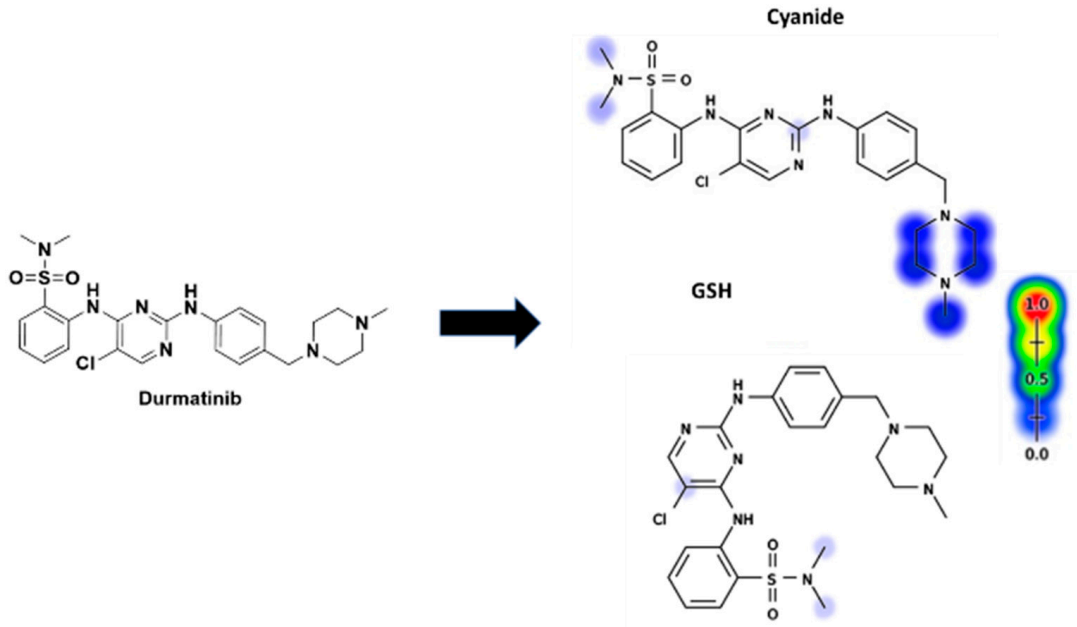

Figure 3. Predicted bioactive sites of DMB by Xenosite web predictor, including GSH and cyano bioactive centers.

3.2. DMB Fragmentation

The parent ion peak (PIP) of DMB appeared at 29.5 min in the total ion chromatogram (TIC) (Figure 4A). PI fragmentation at m/z 516 yielded two daughter ions at m/z 313 and 206 (Figure 4B). The molecular structure of DMB was divided into two parts, labeled A (in red) and B (in blue), to assist in the identification of specific metabolic reactions (Figure 4C).

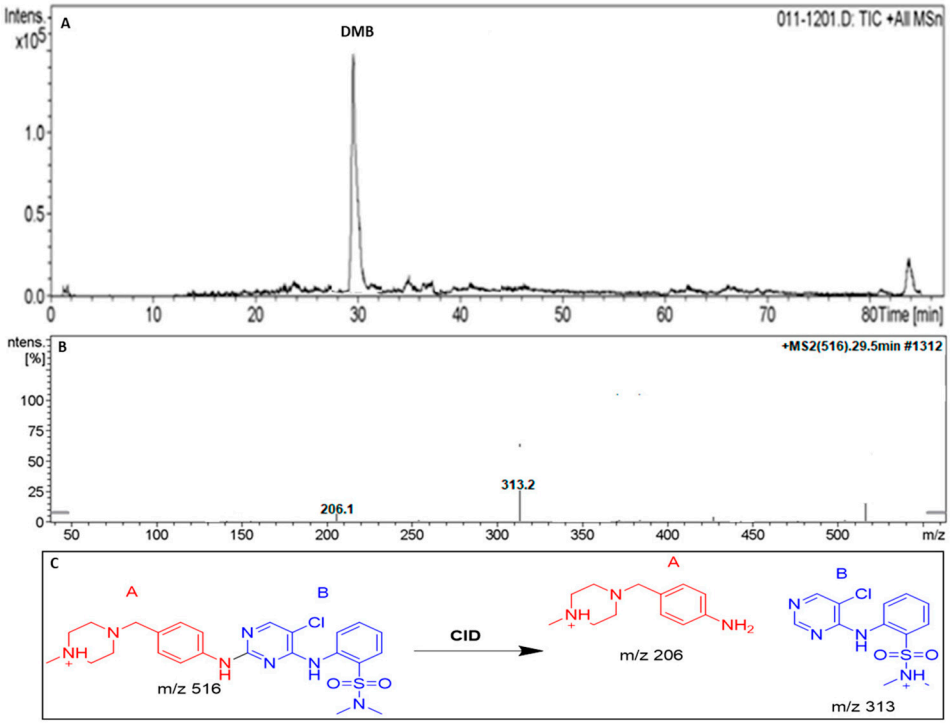

Figure 4. TIC of DMB (**A**). Positive ion MS/MS of DMB at 29.5 min (**B**). Fragment ions of DMB (**C**).

3.3. Phase I Metabolites of DMB Identified In Vitro

There were seven different phase I metabolites identified:

- M1 and M2 (*N*-demethylation metabolites) at (*m*/*z*: 502).
- M3 (*m*/*z* = 474) was found to be the only metabolite with triple *N*-demethylation.
- M4 (*m*/*z* = 532) was shown to be a hydroxylated metabolite.
- M5 at (*m*/*z* = 498), a product of dechlorination and hydroxylation, has been isolated.
- The metabolite M6 at (*m*/*z*: 484) has been shown to undergo *N*-demethylation, dechlorination, and hydroxylation.

One metabolite, designated M7 at (*m*/*z:* 514), was shown to be the product of dechlorination and double hydroxylation (Table 1). Figures S1–S6 (Supplementary File) are provided for M2, M3, M4, M5, M6, and M7. These three metabolic reactions occurred after DMB was incubated with HLMs, resulting in the seven metabolites: *N*-deethylation, *N*-dichloromethylation, and O-hydroxylation [21].

Table 1. Phase I metabolites of DMB identified in MS and MS/MS scans.

	MS Scan	Major Daughter Ions	t_R (min)	Proposed Metabolic Reaction
DMB	516	206,313	29.5	DMB + H
M1	502	313,192	22.7	*N*-demethylation at piperazine ring
M2	502	299,206	23.1	*N*-demethylation at sulphonamide group
M3	474	192,285	24.4	*N*-demethylation at piperazine ring and sulphonamide group
M4	532	313,222,117	25.1	α hydroxylation at piperazine ring
M5	498	295,206,98	27.5	Dechlorination then hydroxylation
M6	484	295.192	28.1	Dechlorination, then hydroxylation and *N*-demethylation at piperazine ring
M7	514	295,222,117	28.6	Dechlorination followed by hydroxylation at pyrimidine and hydroxylation at piperazine ring

3.3.1. The DMB M1 Metabolites Identification

At 22.7 min, we saw the M1 PIP, which indicated DMB *N*-demethylation (Figure 5A). Collision-induced dissociation (CID) fragmented the molecular ion peak (MIP) at *m*/*z* 502, yielding ions at *m*/*z* 313 and 192 (Figure 5B). Similarly to the other fragment ions at *m*/*z* 313, the *m*/*z* 192 daughter ion suggests that the *N*-demethylation occurred at the DMB piperazine ring (Figure 5C).

3.3.2. Identification of the DMB M2 Metabolites

DMBs *N*-demethylation metabolite, M2 PIP, was detected at 23.1 min. Fragment ions at *m*/*z* 299 and 206 were generated by collision-induced dissociation (CID) of the molecular ion peak (MIP) at *m*/*z* 502 (Figure S1A). A daughter ion at *m*/*z* 299 was formed, which matched the other fragment ion at *m*/*z* 206, indicating that the *N*-demethylation occurred at the sulphonamide moiety (part B of DMB) (Figure S1B).

3.3.3. Identification of the DMB M3 Metabolite

At 24.4 min, the *N*-demethylation metabolite of DMB, M3 PIP, was detected. Fragment ions with masses of 285 and 192 were produced through collision-induced dissociation (CID) of the MIP at *m*/*z* 474 (Figure S2A). *N*-demethylation was likely performed on the piperazine ring, as evidenced by the formation of a daughter ion at *m*/*z* 285 (part A of DMB). Another *N*-demethylation process of two methyl groups occurred at the

sulphonamide group (part B DMB), as indicated by the production of a daughter ion at m/z 192 (Figure S2B).

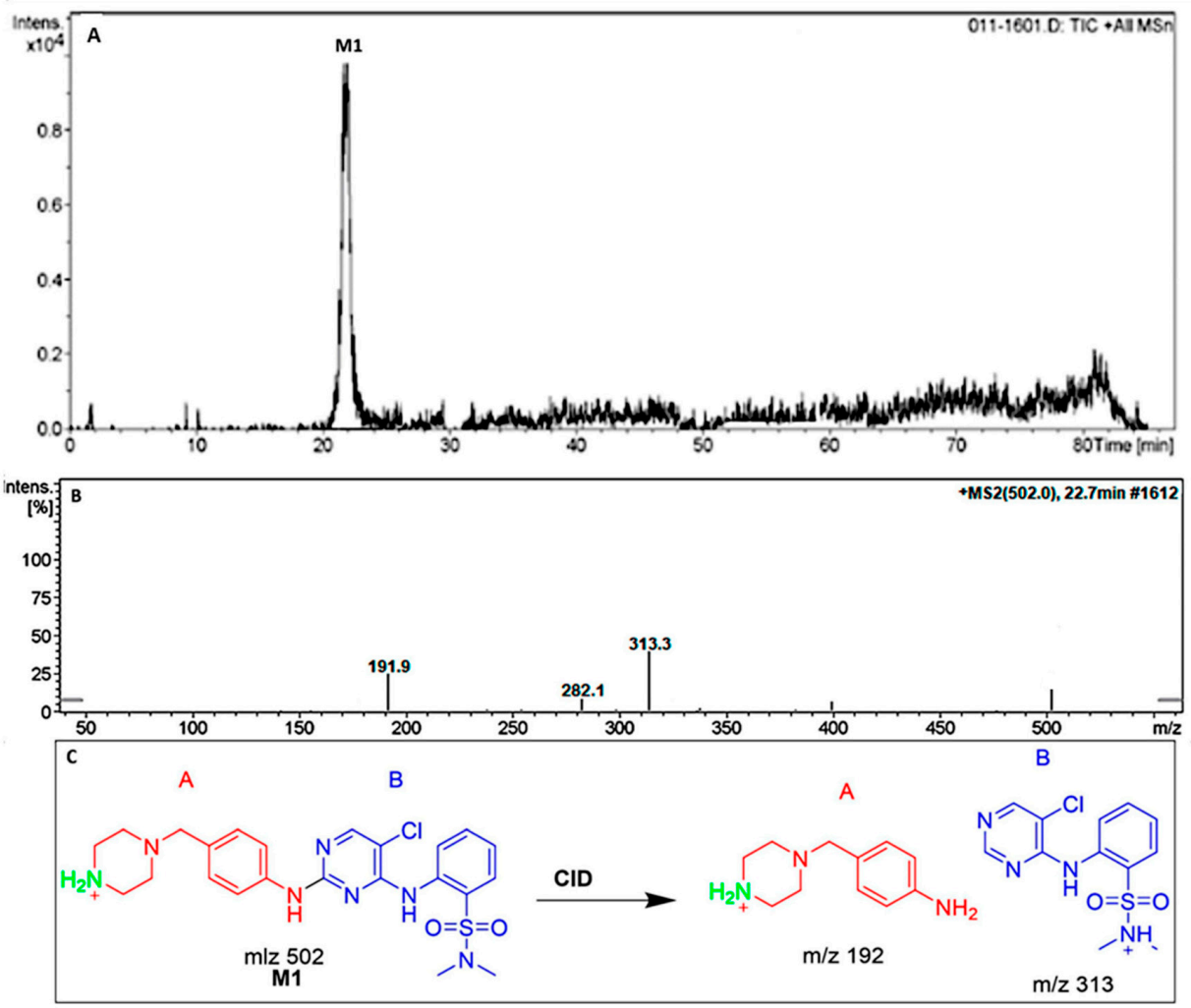

Figure 5. TIC of M1 (**A**). Positive ion MS/MS of M1 at 22.7 min (**B**). Fragment ions of M1 (**C**).

3.3.4. Identification of the DMB M4 Metabolite

At 25.1 min, the DMB hydroxylation metabolite, M4 PIP, was detected. There were fragment ions with m/z values of 313, 222, and 117 generated by the CID of the MIP at m/z 532 (Figure S3A). The m/z 222 daughter ion, along with the m/z 313 and m/z 117 fragment ions, revealed that the hydroxylation happened in the piperazine moiety (part A of DMB) (Figure S3B).

3.3.5. Identification of the DMB M5 Metabolite

Around 27.5 min, the M5 PIP appeared. Dechlorination was followed by hydroxylation of the pyrimidine ring, resulting in the M5 metabolite. There were fragment ions at m/z 295, 206, and 98 produced by the CID of MIP at m/z 498 (Figure S4A). A daughter ion at m/z 295 was formed, which matched the other fragment ions at m/z 206 and m/z 98, indicating that dechlorination followed by a hydroxylation reaction took place at the pyrimidine ring (part B of the DMB structure) (Figure S4B).

3.3.6. Identification of the DMB M6 Metabolite

At 28.1 min, the M6 PIP was detected. *N*-demethylation, dechlorination, and hydroxylation all resulted in the M6 metabolite. Fragment ions with masses of 295 and 192 were produced when CID was applied to MIP at m/z 484 (Figure S5A). Dechlorination and

subsequent hydroxylation reactions, as indicated by the formation of a daughter ion at m/z 295, likely occurred in the pyrimidine ring (region B of the DMB structure) (Figure S5B). As the DMB structure's piperazine ring produced a daughter ion at m/z 192, this indicated that *N*-demethylation had taken place there (Figure S5B).

3.3.7. Identification of the M7 DMB Metabolite

The M6 PIP appeared at 28.6 min. The metabolite M6 was the net product of the dechlorination of the chlorine group and double hydroxylation. The CID of the MIP at m/z 514 generated fragment ions at m/z 295, 222, and 117 (Figure S6A). The production of the daughter ion at m/z 295 indicated the dechlorination followed by hydroxylation reactions occurred at the pyrimidine ring (part B of the DMB structure) (Figure S6B). The production of daughter ions at m/z 222 and 117 suggested that there was another hydroxylation reaction that occurred at the piperazine ring in part A of the DMB structure (Figure S6B).

3.4. Identification of In Vitro DMB Reactive Metabolites

The identical metabolic interaction between DMB and HLMs was carried out to capture iminium and 2,5-quinone-imine intermediates in the presence of 1.0 mM KCN and 1.0 mM GSH, respectively. Bioactivation and subsequent trapping by cyano and GSH nucleophiles of the *N*-methyl piperazine and pyrimidine rings of the DMB structure are illustrated in Table 2 [9,22].

Table 2. DMB reactive metabolites.

	MS Scan	Most Abundant Fragment Ions	R_t (min)	Metabolic Reaction
Cyano adducts				
DMB541CN	541	126, 231, 313, 514	35.2	Attack of KCN at bioactivated *N*-methyl piperazine ring
DMB527CN	527	217, 313, 500	37.0	*N*-demethylation and attack of KCN at bioactivated *N*-methyl piperazine ring.
DMB513CN	513	126, 231, 285	38.1	Double *N*-demethylation at sulphonamide group and attack of KCN at bioactivated *N*-methyl piperazine ring.
GSH conjugates				
DMB803GSH	803	206, 496, 600	41.5	Conjugation of GSH at bioactivated 2,5quinone-imine
DMB789GSH	789	206, 308, 586	42.6	*N*-demethylation at sulphonamide and conjugation of GSH at bioactivated 2,5quinone-imine

3.4.1. Identification of the DMB541CN Cyano Adduct Reactive Metabolite of DMB

After 35.2 min, the DMB541CN PIP was detected (Figure 6A). Cyano nucleophiles may have attacked the bioactivated piperazine ring in DMB541CN during the metabolic reaction that occurred there. Daughter ions at m/z 126, 231, and 313 were produced by the DMB541CN CID at m/z 541 (Figure 6B). The loss of hydrogen cyanide molecules (27 Da) was compatible with the cyano addition, as suggested by the PI at m/z 541. The cyanide adduct was confirmed, and the elimination of the HCN was suggested by a neutral loss at mass m/z 27 (Figure 6C). The cyanide ion was added to the *N*-methyl piperazine ring, as evidenced by the resulting ions at m/z 126, 231, and 313 (Scheme 1).

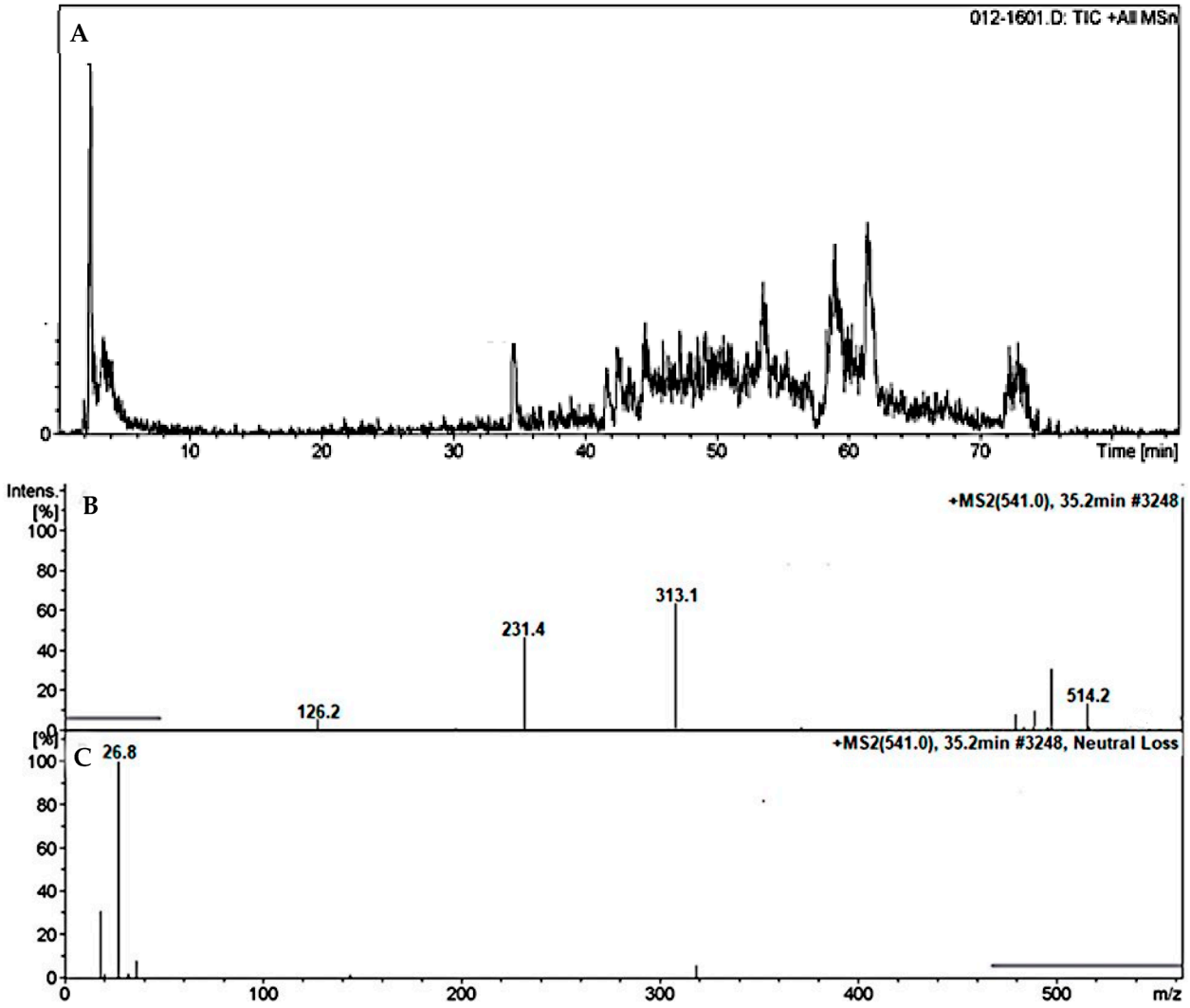

Figure 6. TIC of DMB541CN (**A**). Fragment ions of DMB541CN (**B**). Constant neutral loss scan of DMB541CN (**C**).

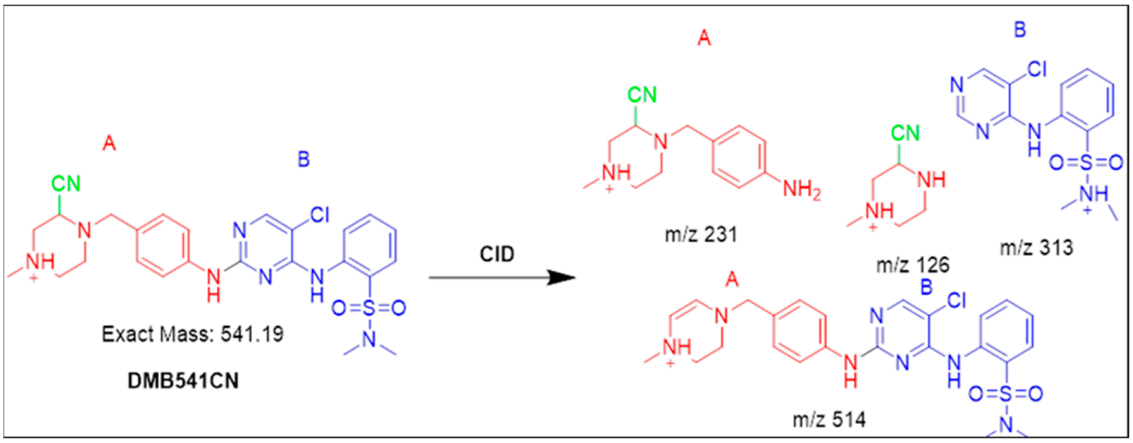

Scheme 1. Fragmentation pattern of DMB541CN $[M + H]^-$ at m/z = 541. The important DMB metabolites; piperazine ring moiety (A) and pyrimidine ring part (B).

3.4.2. Identification of the DMB527CN Cyano Adduct Reactive Metabolite of DMB

At 27 min, a PIP for the DMB527CN was displayed (Figure 7A). *N*-demethylation and the attack of cyano nucleophiles on the bioactivated piperazine ring occurred as metabolic

reactions in DMB527CN, leading to the formation of the cyano adduct. Three distinctive product ions with mass numbers of 500, 313, and 217 were generated when the DMB527CN CID ion was excited at mass number 527 (Figure 7B). As indicated by PI at m/z 500, the loss of hydrogen cyanide molecules (27 Da) was consistent with the cyano addition. The cyanide adduct was confirmed, and the elimination of the HCN was suggested by a neutral loss at mass m/z 27 (Figure 7C). The m/z 313 and 217 ion peaks, when compared to PIs of DMB, showed that the *N*-methyl piperazine ring had been modified by the addition of cyanide (Scheme 2).

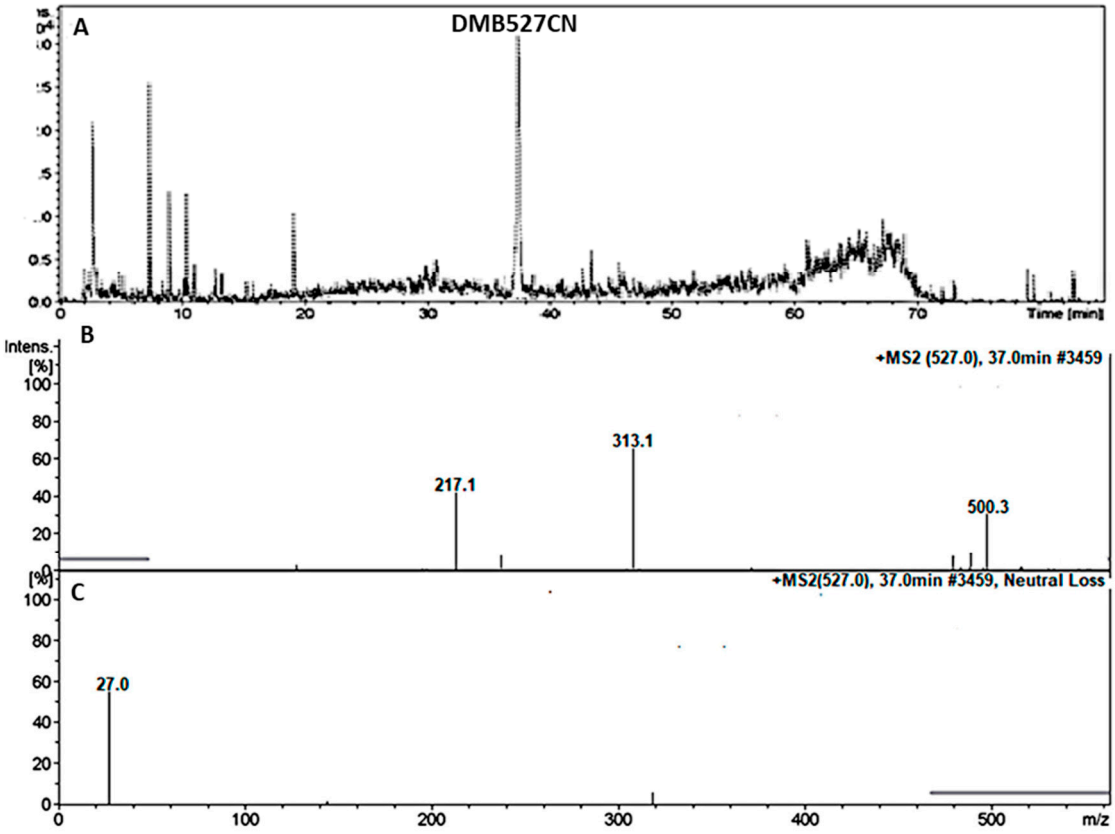

Figure 7. TIC of DMB527CN (**A**). Fragment ions of DMB527CN (**B**). Constant neutral loss scan of DMB527CN (**C**).

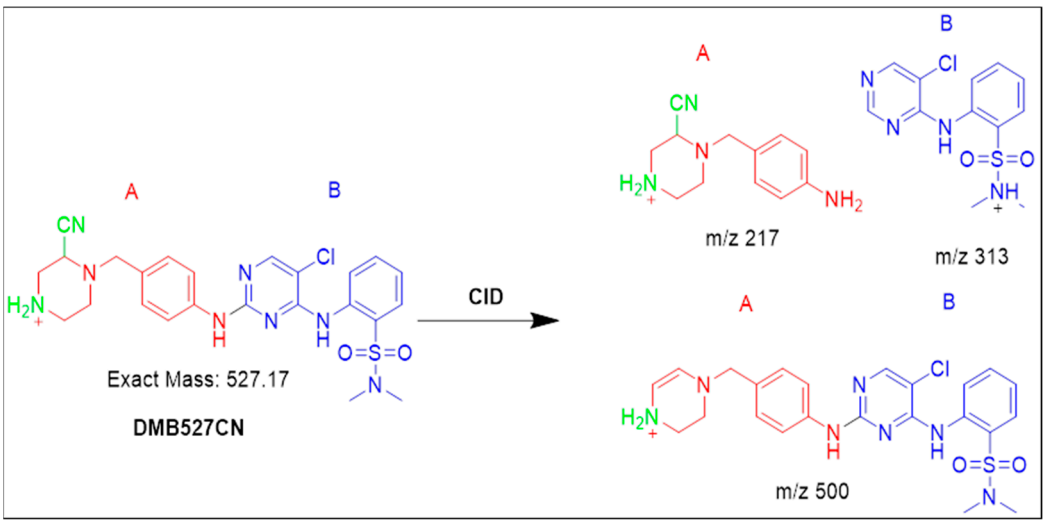

Scheme 2. Fragmentation pattern of DMB527CN $[M + H]^-$ at $m/z = 527$.

3.4.3. Identification of the DMB513CN Cyano Adduct Reactive Metabolite of DMB

At 38.1 min, the DMB513CN appeared (Figure 8A). The metabolic reactions that occurred in DMB513CN suggested that the cyano adduct was afforded by *N*-demethylation at the sulphonamide group and the attacking of cyano nucleophiles on the bioactivated piperazine ring. At m/z 513, four distinct product ions, 486, 213, 126, and 285, were generated through collision-induced dissociation (CID) of the parent DMB513CN ion (Figure 8B). PI at m/z 486 indicates the disappearance of hydrogen cyanide molecules (27 Da). The cyanide adduct was confirmed, and the elimination of the HCN was suggested by a neutral loss at mass m/z 27 (Figure 8C). The addition of cyanide ions at the *N*-methyl piperazine ring was confirmed by the product ions at m/z 126, 231, and 285, which were compared to PIs of DMB (Scheme 3).

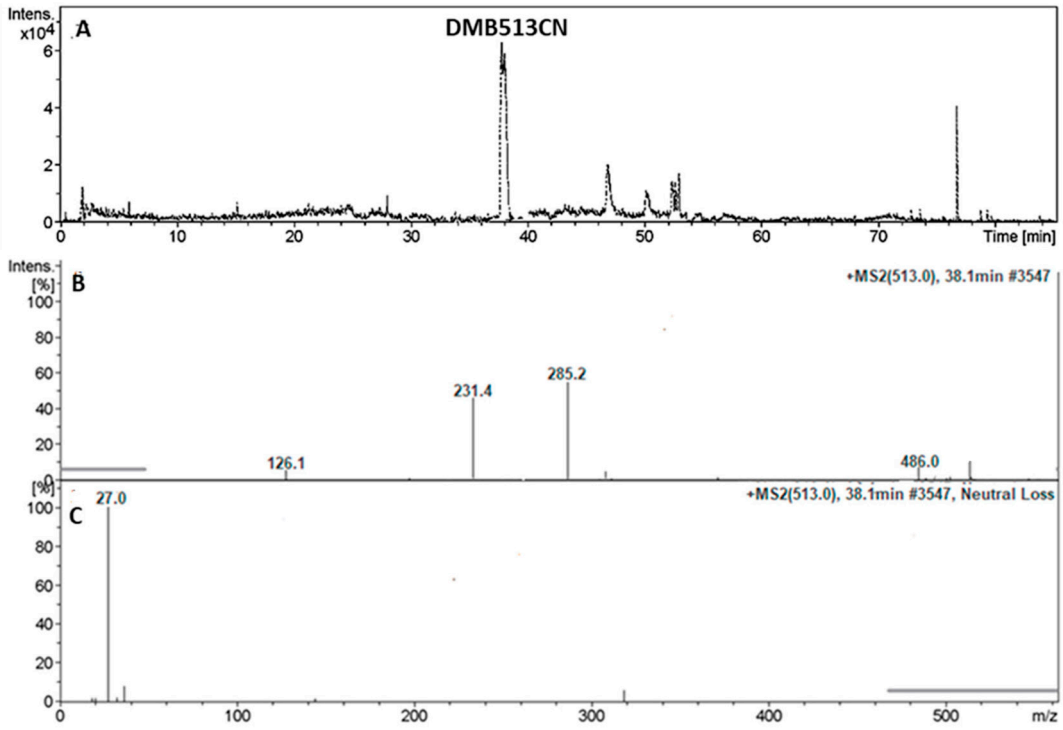

Figure 8. TIC of DMB513CN (**A**). Fragment ions of DMB513CN (**B**). Constant neutral loss scan of DMB513CN (**C**).

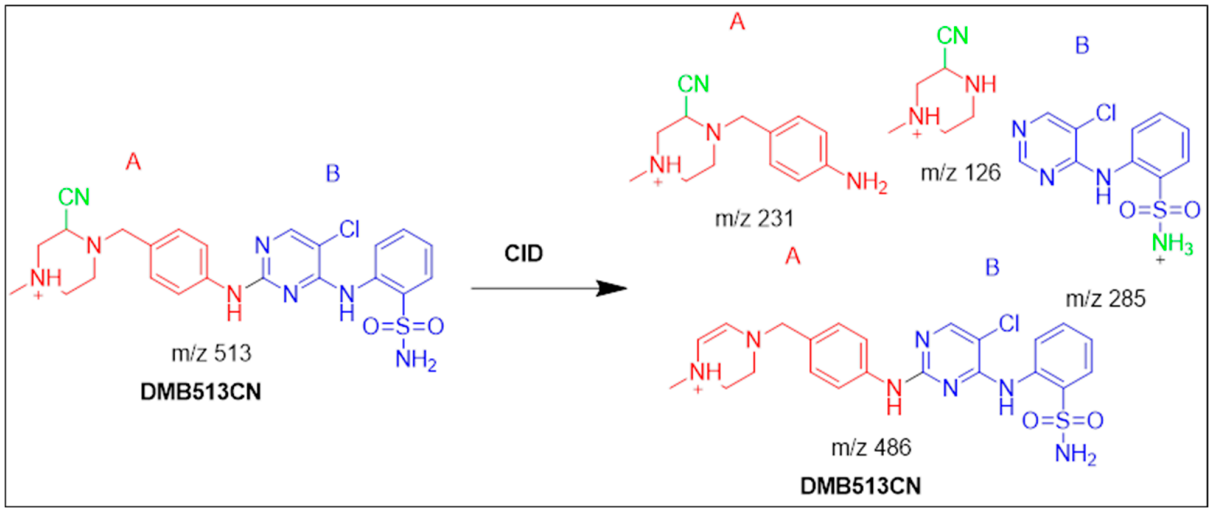

Scheme 3. Fragmentation pattern of DMB513CN $[M + H]^-$ at m/z = 513.

3.5. Identification of DMB GSH Conjugates

3.5.1. Identification of the DMB803GSH Conjugate DMB

At approximately 41.5 min, the appearance of DMB803GSH was observed (Figure 9A). DMB803GSH's metabolic pathways pointed to dechlorination, hydroxylation, and conjugation of GSH at 2,5-quinone-imine (Scheme 4). The production of DMB803GSH from DMB in vitro suggested the formation of 2,5-quinone-imine. DMB803GSH, a CID ion at m/z 803, decomposed into m/z 600, 496, and 206 ions (Figure 9B). The synthesis of conjugated GSH was confirmed by the presence of a molecule ion at m/z 496. In relation to DMB PIs, the resultant ions at m/z 600 and 206 validated the conjugation of GSH at the DMB pyrimidine ring (Scheme 4). Another LC–MS/MS screening for the GSH conjugate was done by constant neutral loss scan monitoring of ions that lost 307 Da (Figure 9C) [23].

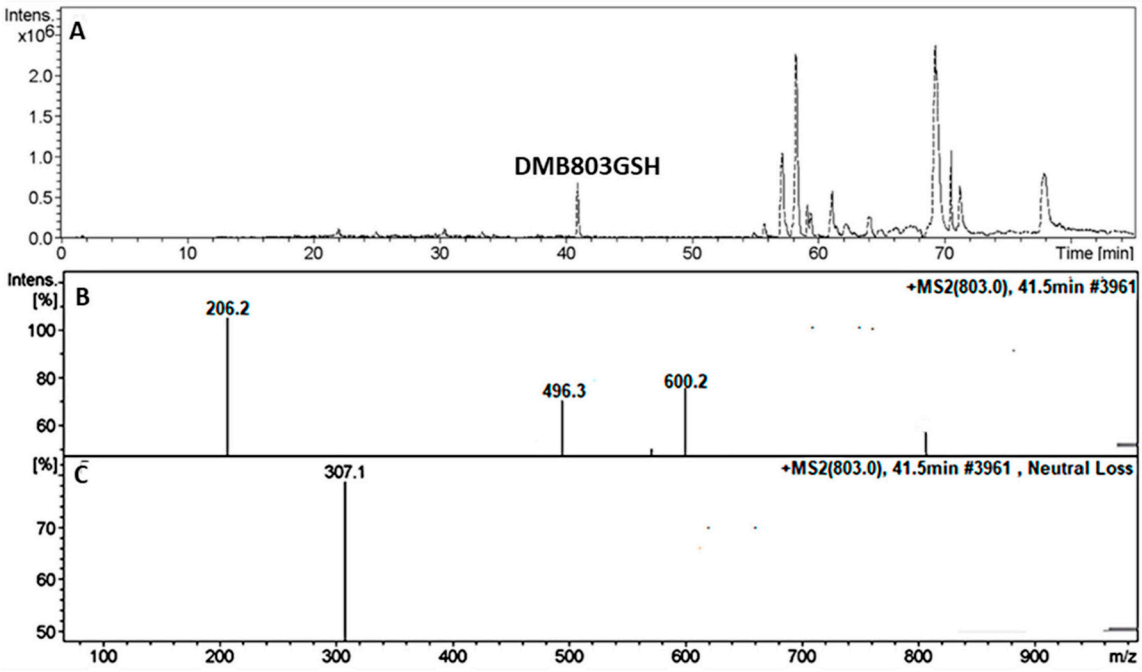

Figure 9. TIC of DMB803GSH (**A**). Fragment ions of DMB803GSH (**B**). Constant neutral loss scan of DMB803GSH (**C**).

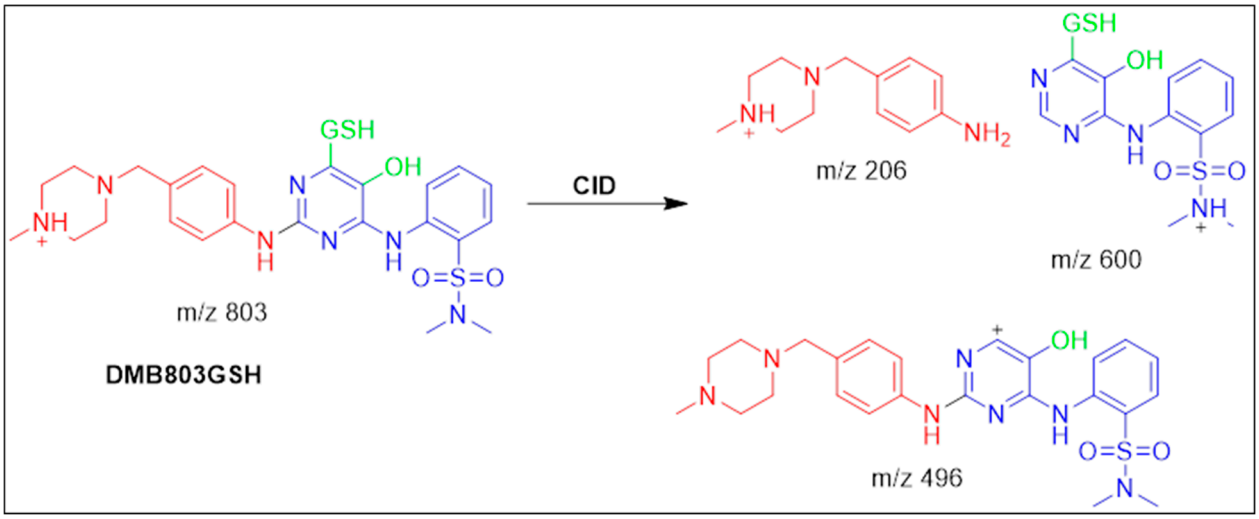

Scheme 4. Fragmentation pattern of DMB803GSH $[M + H]^-$ at m/z = 803.

3.5.2. Identification of the DMB789GSH Conjugate DMB

At 42.6 min, the DMB789GSH started to appear (Figure 10A). The metabolic pathways that were active in DMB789GSH were anticipated to be *N*-demethylation at the sulphonamide group, dechlorination, hydroxylation, and GSH conjugation at the 2,5-quinone-imine (Scheme 5). In vitro DMB metabolism, as evidenced by the production of DMB789GSH, resulted in the synthesis of 2,5-quinone-imine. The m/z 789 DMB789GSH CID ion decomposed into four m/z 660, 586, 308, and 206 fragment ions (Figure 10B). Pyroglutamic acid cleavage yields an ion at m/z 660 (129 Da) that agrees with a GSH conjugation being generated (Scheme 5). The m/z 586 and m/z 206 ionic fragments of the same molecule revealed GSH conjugation at the DMB pyrimidine ring and hence their relationship to PIs of DMB (Figure 10B). The m/z 308 resultant ion represents the dissociation of GSH conjugation (Figure 10C). Constant neutral loss scan monitoring of ions that lost 307 Da was used in another round of LC-MS/MS screening for the GSH conjugate (Figure 10C) [22].

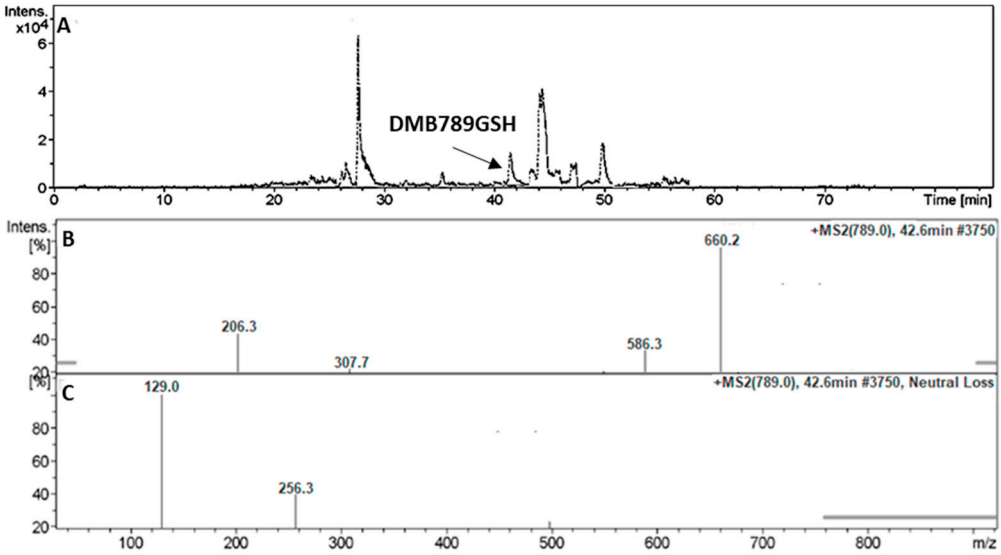

Figure 10. TIC of DMB789GSH (**A**). Fragment ions of DMB789GSH (**B**). Constant neutral loss scan of DMB789GSH (**C**).

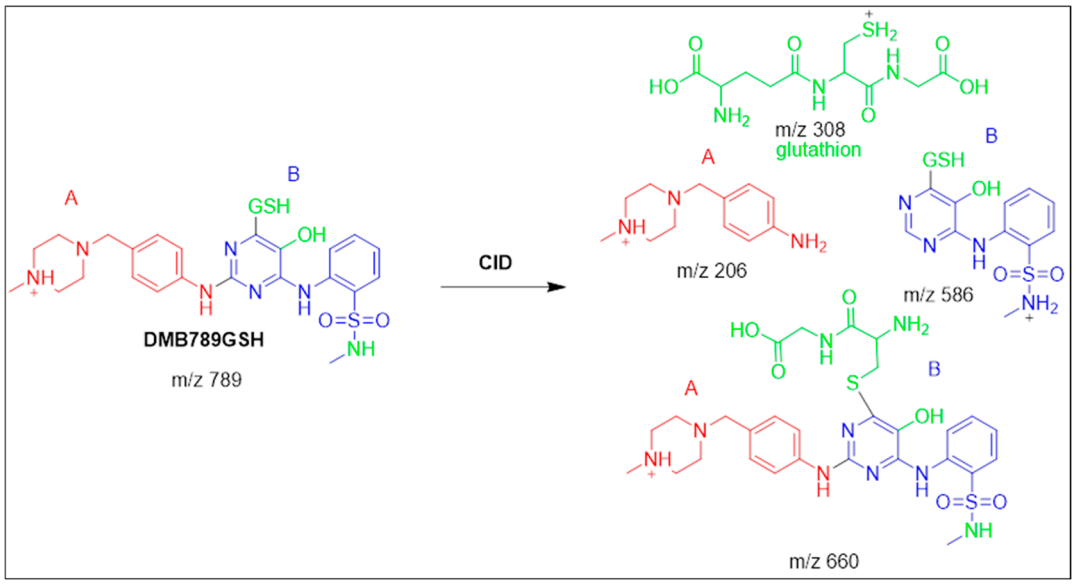

Scheme 5. Fragmentation pattern of DMB789GSH $[M + H]^-$ at $m/z = 789$.

3.6. Proposed Bioactivation Pathways of DMB

Figure 11 depicts possible bioactivation pathways for DMB. Cyanide adducts (DMB541CN, DMB527CN, and DMB513CN) detected in DMB during metabolism suggested that iminium intermediates were formed at the *N*-methyl piperazine ring. It was hypothesized that the bioactivation mechanism involved hydroxylation at DMB *N*-methyl piperazine, followed by dehydration, to produce the iminium ion intermediate as a highly reactive and unstable nucleophile. To isolate these reactive intermediates, KCN was used, and LC-MS was then used to identify the stable cyanide adducts that resulted. The bioactive mechanism of the iminium intermediate [9,14,21] has been studied using cyclic tertiary amine-containing drugs. In order to validate the formation of 2,5-quinone-imine intermediates in DMB metabolism, glutathione (GSH) was used as a trapping agent. We anticipated that GSH-producing conjugates like DMB803GSH and DMB789GSH [9,24] might target the bioactivation process comprising dechlorination, hydroxylation, and oxidation to produce 2,5-quinone-imine (Figure 11).

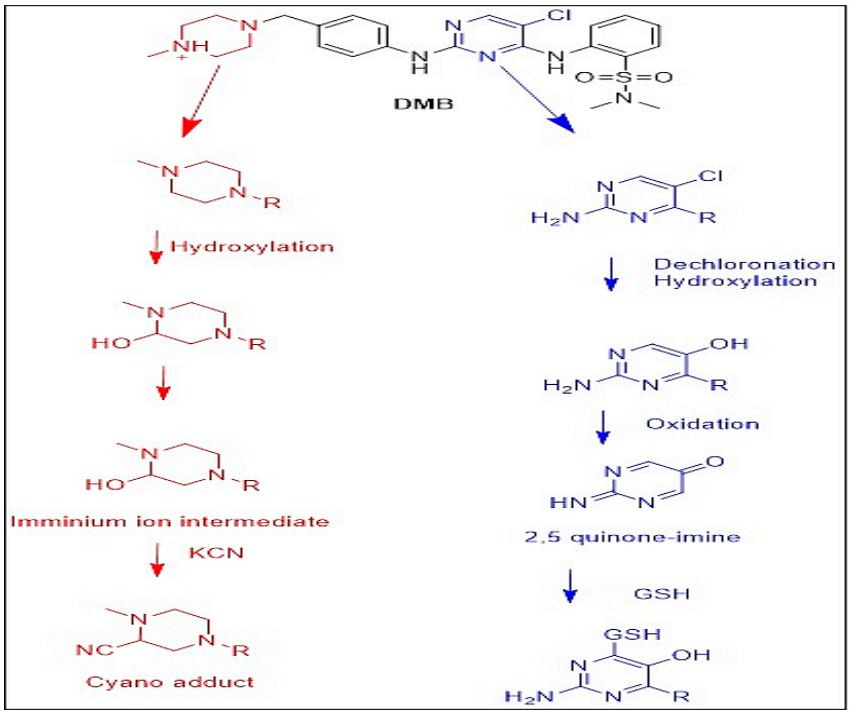

Figure 11. Proposed pathways for DMB bioactivation.

4. Conclusions

In this study, we successfully identified seven phase I metabolites of DMB through in vitro analysis. These metabolites were generated as a result of *N*-demethylation, hydroxylation, and dechlorination reactions. Notably, our findings revealed the presence of five reactive metabolites, including three cyano adducts and two GSH conjugates. To assess the potential toxicity, we employed the Xenosite web-based predictor to perform in silico predictions on DMB and its metabolites. Our results shed light on the previously assumed role of metabolism and bioactivation reactions at the pyrimidine and piperazine rings, which were considered responsible for DMBs toxicity and instability.

Supplementary Materials: The following supporting information can be downloaded at: https://www.mdpi.com/article/10.3390/separations10060353/s1, Figure S1: Positive ion MS/MS mass spectrum of M2 at 23.1 min (A). Proposed structural formulas of M2 and corresponding MS/MS fragments (B); Figure S2: Positive ion MS/MS mass spectrum of M3 at 24.4 min (A). Proposed structural formulas of M3 and corresponding MS/MS fragments (B); Figure S3: Positive ion MS/MS mass spectrum of M4 (A). Proposed structural formulas of M4 and corresponding MS/MS fragments (B); Figure S4:

Positive ion MS/MS mass spectrum of M5 at 27.5 min (A). Proposed structural formulas of M5 and corresponding MS/MS fragments (B); Figure S5: Positive ion MS/MS mass spectrum of M6 at 28.1 min (A). Proposed structural formulas of M6 and corresponding MS/MS fragments (B); Figure S6: Positive ion MS/MS mass spectrum of M7 at 28.6 min (A). Proposed structural formulas of M7 and its corresponding MS/MS fragments (B).

Author Contributions: Writing original draft, investigation, and data curation, N.S.A.-S.; writing-reviewing H.A.A., A.A.K. and R.A.-S. All authors have read and agreed to the published version of the manuscript.

Funding: This work was funded by Deputyship for Research and Innovation, Ministry of Education, Saudi Arabia via project no. (IFKSUOR3–347-1).

Data Availability Statement: Not applicable.

Acknowledgments: The authors extend their appreciation to the Deputyship for Research and Innovation, Ministry of Education in Saudi Arabia, for funding this research work through project no. (IFKSUOR3–347-1).

Conflicts of Interest: The authors declare that they have no known competing financial interest or personal relationship that could have appeared to influence the work reported in this paper.

Abbreviations

CAN: acetonitrile; CID: collision-induced dissociation; DMB: Dubermatinib; ESI: electrospray ionization; HLMs: human liver microsomes; LC-MS, liquid chromatography ion trap mass spectrometry; PIP: parent ion peak; TIC: total ion chromatogram; TKIs: tyrosine kinase inhibitors. SOM: site of metabolism.

References

1. Natoli, C.; Perrucci, B.; Perrotti, F.; Falchi, L.; Iacobelli, S. Tyrosine Kinase Inhibitors. *Curr. Cancer Drug Targets* **2010**, *10*, 462–483. [CrossRef] [PubMed]
2. Lemmon, M.A.; Schlessinger, J. Cell Signaling by Receptor Tyrosine Kinases. *Cell* **2010**, *141*, 1117–1134. [CrossRef] [PubMed]
3. Tanaka, M.; Siemann, D.W. Therapeutic Targeting of the Gas6/Axl Signaling Pathway in Cancer. *Int. J. Mol. Sci.* **2021**, *22*, 9953. [CrossRef] [PubMed]
4. Sinha, S.; Boysen, J.C.; Chaffee, K.G.; Kabat, B.F.; Slager, S.L.; Parikh, S.A.; Secreto, C.R.; Call, T.; Shanafelt, T.D.; Leis, J.F. Chronic Lymphocytic Leukemia Cells from Ibrutinib Treated Patients Are Sensitive to Axl Receptor Tyrosine Kinase Inhibitor Therapy. *Oncotarget* **2018**, *9*, 37173. [CrossRef]
5. Sen, T.; Tong, P.; Diao, L.; Li, L.; Fan, Y.; Hoff, J.; Heymach, J.V.; Wang, J.; Byers, L.A. Targeting AXL and MTOR Pathway Overcomes Primary and Acquired Resistance to WEE1 Inhibition in Small-Cell Lung CancerAXL/MTOR–Mediated WEE1 Inhibitor Resistance in SCLC. *Clin. Cancer Res.* **2017**, *23*, 6239–6253. [CrossRef]
6. Aveic, S.; Corallo, D.; Porcù, E.; Pantile, M.; Boso, D.; Zanon, C.; Viola, G.; Sidarovich, V.; Mariotto, E.; Quattrone, A. TP-0903 Inhibits Neuroblastoma Cell Growth and Enhances the Sensitivity to Conventional Chemotherapy. *Eur. J. Pharmacol.* **2018**, *818*, 435–448. [CrossRef]
7. Li, F.; Lu, J.; Ma, X. Profiling the Reactive Metabolites of Xenobiotics Using Metabolomic Technologies. *Chem. Res. Toxicol.* **2011**, *24*, 744–751. [CrossRef]
8. Al-Shakliah, N.S.; Attwa, M.W.; Kadi, A.A.; AlRabiah, H. Identification and Characterization of In Silico, In Vivo, In Vitro, and Reactive Metabolites of Infigratinib Using LC-ITMS: Bioactivation Pathway Elucidation and in Silico Toxicity Studies of Its Metabolites. *RSC Adv.* **2020**, *10*, 16231–16244. [CrossRef]
9. Bolton, J.L.; Trush, M.A.; Penning, T.M.; Dryhurst, G.; Monks, T.J. Role of Quinones in Toxicology. *Chem. Res. Toxicol.* **2000**, *13*, 135–160. [CrossRef]
10. Ma, S.; Zhu, M. Recent Advances in Applications of Liquid Chromatography–Tandem Mass Spectrometry to the Analysis of Reactive Drug Metabolites. *Chem. Biol. Interact.* **2009**, *179*, 25–37. [CrossRef]
11. Stepan, A.F.; Walker, D.P.; Bauman, J.; Price, D.A.; Baillie, T.A.; Kalgutkar, A.S.; Aleo, M.D. Structural Alert/Reactive Metabolite Concept as Applied in Medicinal Chemistry to Mitigate the Risk of Idiosyncratic Drug Toxicity: A Perspective Based on the Critical Examination of Trends in the Top 200 Drugs Marketed in the United States. *Chem. Res. Toxicol.* **2011**, *24*, 1345–1410. [CrossRef] [PubMed]
12. Tolonen, A.; Turpeinen, M.; Pelkonen, O. Liquid Chromatography–Mass Spectrometry in in Vitro Drug Metabolite Screening. *Drug Discov. Today* **2009**, *14*, 120–133. [CrossRef]

13. Attwa, M.W.; Kadi, A.A.; Darwish, H.W.; Amer, S.M.; Al-Shakliah, N.S. Identification and Characterization of in Vivo, in Vitro and Reactive Metabolites of Vandetanib Using LC–ESI–MS/MS. *Chem. Cent. J.* **2018**, *12*, 99. [CrossRef] [PubMed]
14. DiMasi, J.A.; Hansen, R.W.; Grabowski, H.G. The Price of Innovation: New Estimates of Drug Development Costs. *J. Health Econ.* **2003**, *22*, 151–185. [CrossRef] [PubMed]
15. Raies, A.B.; Bajic, V.B. In Silico Toxicology: Computational Methods for the Prediction of Chemical Toxicity. *Wiley Interdiscip. Rev. Comput. Mol. Sci.* **2016**, *6*, 147–172. [CrossRef]
16. Matlock, M.K.; Hughes, T.B.; Swamidass, S.J. XenoSite Server: A Web-Available Site of Metabolism Prediction Tool. *Bioinformatics* **2015**, *31*, 1136–1137. [CrossRef]
17. Zaretzki, J.; Matlock, M.; Swamidass, S.J. XenoSite: Accurately Predicting CYP-Mediated Sites of Metabolism with Neural Networks. *J. Chem. Inf. Model.* **2013**, *53*, 3373–3383. [CrossRef]
18. Dang, N.L.; Hughes, T.B.; Krishnamurthy, V.; Swamidass, S.J. A Simple Model Predicts UGT-Mediated Metabolism. *Bioinformatics* **2016**, *32*, 3183–3189. [CrossRef]
19. Jia, L.; Liu, X. The Conduct of Drug Metabolism Studies Considered Good Practice (II): In Vitro Experiments. *Curr. Drug Metab.* **2007**, *8*, 822–829. [CrossRef]
20. Al-Shakliah, N.S.; Attwa, M.W.; AlRabiah, H.; Kadi, A.A. Identification and Characterization of in Vitro, in Vivo, and Reactive Metabolites of Tandutinib Using Liquid Chromatography Ion Trap Mass Spectrometry. *Anal. Methods* **2021**, *13*, 399–410. [CrossRef]
21. Al-Shakliah, N.; Kadi, A.; Al-Salahi, R.; Rahman, A.F.M. In Vitro Identification of Potential Metabolites of Plinabulin (NPI 2358) in Hepatic Preparations Using Liquid Chromatography–Ion Trap Mass Spectrometry. *ACS Omega* **2022**, *7*, 21465–21472. [CrossRef] [PubMed]
22. Jian, W.; Liu, H.-F.; Zhao, W.; Jones, E.; Zhu, M. Simultaneous Screening of Glutathione and Cyanide Adducts Using Precursor Ion and Neutral Loss Scans-Dependent Product Ion Spectral Acquisition and Data Mining Tools. *J. Am. Soc. Mass Spectrom.* **2012**, *23*, 964–976. [CrossRef] [PubMed]
23. Xie, C.; Zhong, D.; Chen, X. A Fragmentation-Based Method for the Differentiation of Glutathione Conjugates by High-Resolution Mass Spectrometry with Electrospray Ionization. *Anal. Chim. Acta* **2013**, *788*, 89–98. [CrossRef] [PubMed]
24. Abdelhameed, A.S.; Attwa, M.W.; Kadi, A.A. Characterization of Stable and Reactive Metabolites of the Anticancer Drug, Ensartinib, in Human Liver Microsomes Using LC-MS/MS: An in Silico and Practical Bioactivation Approach. *Drug Des. Devel. Ther.* **2020**, *14*, 5259. [CrossRef]